Journal Pre-proof

Study of acidic degradation of alkali-activated materials using synthetic C-(N)-A-S-H and N-A-S-H gels

Yanru Wang, Yubin Cao, Zuhua Zhang, Jizhong Huang, Peng Zhang, Yuwei Ma, Hao Wang

PII: S1359-8368(21)00877-5

DOI: https://doi.org/10.1016/j.compositesb.2021.109510

Reference: JCOMB 109510

To appear in: *Composites Part B*

Received Date: 8 September 2021

Revised Date: 27 October 2021

Accepted Date: 20 November 2021

Please cite this article as: Wang Y, Cao Y, Zhang Z, Huang J, Zhang P, Ma Y, Wang H, Study of acidic degradation of alkali-activated materials using synthetic C-(N)-A-S-H and N-A-S-H gels, *Composites Part B* (2021), doi: https://doi.org/10.1016/j.compositesb.2021.109510.

AUTHORSHIP STATEMENT

Manuscript title: **Study of acidic degradation of alkali-activated materials using synthetic C-(N)-A-S-H and N-A-S-H gels**

Authorship contributions:

Yanru Wang: Conceptualization, Methodology, Investigation, Writing - original draft, Writing - review & editing.

Yubin Cao: Methodology, Conceptualization, Investigation, Writing - review & editing.

Zuhua Zhang: Conceptualization, Supervision, Investigation, Writing - review & editing.

Jizhong Huang: Investigation.

Peng Zhang: Investigation, Writing - review & editing.

Yuwei Ma: Methodology, Investigation, Writing - review & editing.

Hao Wang: Supervision, Investigation, Writing - review & editing.

Study of acidic degradation of alkali-activated materials using synthetic C-(N)-A-S-H and N-A-S-H gels

Yanru Wang[a], Yubin Cao[a], Zuhua Zhang[b, c*], Jizhong Huang[d], Peng Zhang[e], Yuwei Ma[f*], Hao Wang[a*]

[a]*Centre for Future Materials, University of Southern Queensland, Toowoomba, QLD 4350, Australia*

[b]*Key Laboratory for Green & Advanced Civil Engineering Materials and Application Technology of Hunan Province, College of Civil Engineering, Hunan University, Changsha 410082, PR China*

[c]*Key Laboratory of Building Safety and Energy Efficiency of Ministry of Education, Hunan University, Changsha 410082, China*

[d]*Institute for the Conservation of Cultural Heritage, Shanghai University, Shanghai 200444, China*

[e] *School of Civil Engineering, Qingdao University of Technology, Qingdao, 266033, PR China*

[f] *Research Center for Wind Engineering and Engineering Vibration, Guangzhou University, Guangzhou 510006, China*

E-mails of corresponding authors: zuhuazhang@hnu.edu.cn; yuwei_ma@gzhu.edu.cn; hao.wang@usq.edu.au

Abstract:

Alkali-activated materials (AAMs) are usually recognized having better acid resistance compared to ordinary Portland cement (OPC), however, the detailed mechanism has not been well studied due to the complexity of raw materials and hardened matrix. In this study, two typical binding gels in AAMs, sodium aluminum silicate hydrate (N-A-S-H) and calcium (sodium) aluminum silicate hydrate (C-(N)-A-S-H), were chemically prepared by laboratory synthesized aluminosilicate powders. The microstructure and composition evolution of the two gels exposed to sulfuric acid were investigated. The results showed that the C-(N)-A-S-H gel had higher degree of structural order than the N-A-S-H gel, while the N-A-S-H gel showed higher polymerization. The Al^{IV} in N-A-S-H gel transferred completely to Al^{V} during sulfuric acid attack, while trace amount of Al^{IV} was still detected in the exposed C-(N)-A-S-H gels. Both gels had increased silica polymerization degree after exposure to sulfuric acid solution. Due to rapider dealumination of N-A-S-H gel than C-(N)-A-S-H gel, the Si/Al ratio increased much higher in the former. The molecular framework changes of N-A-S-H gel caused by dealumination was found to have less effect on the integrity though than that of C-(N)-A-S-H gel, in which coarse gypsum crystalline grains formed and led to destructive stress in hardened

matrix. This paper provides an insight at microstructure level of the two typical gels, which is essential for the manufacturing and application of alkali-activated materials.

Key words: alkali-activated materials; acid resistance; aluminosilicates; N-A-S-H; C-(N)-A-S-H; durability

1. Introduction

Durability of cementitious materials is an important property due to the growing demand for long-service-life of structures but with low maintenance cost. Concrete is an alkaline material with an initial pH of pore solution around 13, which helps to protect the steel bar in concrete from corrosion [1, 2]. The corrosion of reinforced concrete is dominated by acid-base reactions, causing pH reduction inside concrete, which will further accelerate the acid corrosion of steel bars and hydration products of concrete [3]. Acidic environment also occurs in geothermal wells and groundwater, causing degradation to the underground concrete structures [4]. Among various acidic conditions, sulfuric acid corrosion is considered to be the major cause for acidic degradation of concrete structures [5]. Alkali-activated materials (AAMs), also widely called geopolymers, have emerged as promising environmentally friendly cementitious materials due to the low carbon dioxide emissions and waste utilization in manufacturing [6]. In comparison to ordinary Portland cement (OPC), AAMs usually contain much higher alkali concentration, and perform better in terms of mass change and compressive strength change when subjected to acid attack [7]. However, the detailed corrosion mechanism of AAMs is not clear due to the complexity of raw materials and activators and the product variation.

The acid resistance of cementitious materials is strongly dependent on the interaction between hydration products and acidic media [8]. Hardened OPC-based materials are composed of hydration products calcium hydroxide (CH) and calcium silicate hydrate (C-S-H) gel [9], whereas AAMs are composed of N-A-S-H, C-(N)-A-S-H and their blends, depending on the aluminosilicate materials [10]. While the N-A-S-H gel is known as a three-dimensional alkali aluminosilicate hydrate gel network, consisting of crosslinked [AlO_4] and [SiO_4] tetrahedra linked via shared oxygen atoms, with terminal hydroxyl groups on the gel surface [11]. It is generally described as an amorphous, nanocrystalline zeolite phase [12]. The N-A-S-H gel usually presents ratios of $0.1 \leq Na/Si \leq 0.3$ and $1 \leq Si/Al \leq 4$ [13, 14]. The C-(N)-A-S-H gel is described as an imperfect crosslinked/non-crosslinked Tobermorite-like structure, assembled by two one-dimensional Si tetrahedron chains (randomly Al substitution into paired

tetrahedron) and a calcium octahedron chain [15, 16]. The C-(N)-A-S-H type gel formed in alkali-activated slag possesses a relatively low calcium content [Ca/(Si + Al) < 1.5] compared to the C-S-H gels formed in OPC ($1.5 \leq Ca/Si \leq 2$) [17, 18], and the Al/Si is usually less than or equal to 0.2 [19]. Alkali cations, such as Na^+, are incorporated into C-(N)-A-S-H/N-A-S-H gel via a charge balancing mechanism, where they exist in the interlayer charge-balancing $[AlO_4]^{5-}$ tetrahedra as well as adsorbed to the surface of gel [20]. Understanding the stability of the molecular composition and microstructure evolution of C-(N)-A-S-H/N-A-S-H phases exposed to aggressive environment is critical for the application of AAMs, especially their durability.

Previous researches have attempted to reveal the effects of many factors (i.e. precursors, activators, sample size, acid type, etc.) on acid resistance of AAMs [5, 21-24]. It was reported that sulfuric acid attack caused weight increment and volume expansion of alkali-activated slag (C-(N)-A-S-H is the dominant binding gel), while minor weight and appearance change for alkali-activated fly ash (N-A-S-H is the dominant binding gel) [25]. This is due to the formation of gypsum for high calcium alkali-activated binders. Higher residual compressive strength of alkali-activated slag after acid corrosion was found comparing to alkali-activated fly ash [7, 26]. During the acid attack, the alkali-activated fly ash binder showed leaching of aluminum, sodium, and calcium except for silicon [27]. It is hypothesized that a silicon-rich porous structure was left after acid corrosion in samples. However, elements leaching in acid solution caused a minor change of compressive strength, which proved that this silicon-rich structure contributed most source of the compressive strength in low calcium system [27, 28]. This phenomenon differs from acid attack on OPC.

Decalcification of the binding gels (i.e. C-S-H or C-(N)-A-S-H) has been identified in the both OPC and alkali-activated slag after exposed to acid. The exposed layer of OPC is highly porous silica-rich gel while an aluminosilicate type gel is formed in the affected area of the activated slag sample, and the latter was less soluble and more mechanically sound [29]. Acid attack on fly ash based geopolymer resulted in the substitution of Na^+ and K^+ ions by H^+ or H_3O^+, breaking Si-O-Al and Si-O-Si bonds in N-A-S-H gel, releasing silicic acid [30]. N-A-S-H gel was found to have good stability though [20]. The free sodium existing in the pore solution of the sample can easily diffuse into the external environment. However, acidic corrosion is a complex process. The impacts of contaminates such as iron, carbon, sulfur, etc. are inevitable but none has been illustrated and fully understood [31].

The overall aim of this work is to distinguish the acid corrosion mechanisms of N-A-S-H and C-(N)-A-S-H gels. To avoid those possible effects of contaminants from industrial wastes and keep the same alkali activation procedure for AAM manufacturing, pure precursors were designed and synthesized in the laboratory. After activation by alkali solution, stoichiometric controlled AAM gels, i.e. N-A-S-H and C-(N)-A-S-H, were obtained. The experiment illustrated the evolution of the molecular structure of the gels, particularly the bond change after exposure to H_2SO_4 solution. This work is expected to provide knowledge on improving the acid resistance and application for AAMs as new construction materials.

2. Experimental methods

2.1 Geopolymer binder synthesis

The aluminosilicate powder and calcium-aluminosilicate powder used in this study were synthesized via an organic steric entrapment solution-polymerization route [32]. The precursor compositions (empirical formula $1.5SiO_2 \cdot Al_2O_3$) was chosen to represent the range of bulk silicon and aluminium content typically found in fly ashes [11]. Another precursor (empirical formula $1.07CaO \cdot SiO_2 \cdot 0.086Al_2O_3$) was chosen to enable synthesis of binders exhibiting chemistry range in regions of the calcium aluminium-substituted silicate hydrated gels in alkali-activated slag [11]. The activating solution was prepared by the dissolution of sodium hydroxide powders (Sigma-Aldrich, 98 wt.% purity) in sodium silicate solution (Na_2O = 14.7% (mass), SiO_2 = 29.4%, D-Grade^{TM}, PQ Australia) and distilled water with desired modulus (Ms = SiO_2/Na_2O) of 1. The stoichiometry was designed to obtain a cation ratio of the reaction mixture like the Na_2O-Al_2O_3-SiO_2-H_2O (N-A-S-H) gel and CaO-(Na_2O)-Al_2O_3-SiO_2-H_2O [C-(N)-A-S-H] gel, the reaction products of alkali-activated fly ash and alkali-activated slag, respectively [11] (see Table 1). The activating solutions were mixed with the aluminosilicate powder and calcium aluminosilicate powder in casting containers to form the homogeneous pastes, which are denoted as NASH sample and C(N)ASH sample, respectively. The pastes were stayed in containers (cylinders with diameter of 10 mm and height of 20 mm) with sealed lid and cured at ambient temperature for 120 days. The water/solid ratios (w/s) used for NASH sample and C(N)ASH sample were 1.0 and 0.75, respectively, to obtain a workable and homogeneous paste.

Table 1 Molar ratios in the precursor powder and the reaction mixture for NASH sample and C(N)ASH sample.

Sample ID	Empirical formula	Precursor powder		Reaction mixture			
		Si/Al	Ca/Al	w/s	Si/Al	Na/Al	Ca/(Al + Si)
NASH	$1.5SiO_2 \cdot Al_2O_3$	0.75	0.00	1.00	1.13	0.75	0.00
C(N)ASH	$1.070CaO \cdot SiO_2 \cdot 0.086Al_2O_3$	5.81	4.65	0.75	7.18	1.59	0.57

2.2 Acid corrosion testing procedures

Acid corrosion test was conducted based on the general guidelines in ASTM C267. Following 120 days of sealed curing at 25 °C, five specimens from each mix were submerged in 5 containers with 5% sulfuric acid solution (H_2SO_4) at a liquid to sample mass ratio of 6, respectively. Another five samples were submerged into distilled water as references. The specimens were taken out from the leachates after 1 d, 3 d, 7 d, 28 d and 56 d, respectively. Visual inspection was carried out on each sample. The leaching behavior of each sample had been monitored by recording the pH and elemental concentrations of the distilled water and the 5% sulfuric acid solutions during 56-day immersion of samples. Then the samples were dried overnight in a vacuum oven at 40 °C. The mass loss of samples was calculated by Eq. 1.

$$\Delta m = \frac{m_o - m_c}{m_o} \times 100\% \qquad \text{Eq. 1}$$

where: Δm (%) is the mass change of the specimen during corrosion; m_o is the mass of the dried specimen before corrosion; m_c is the mass of the dried specimen after corrosion.

Inductively coupled plasma mass spectrometry (Thermo X-series II ICP-MS with a CETAC - 500 auto-sampler) was used to analyse the immersion solutions of each sample to determine elements leached from the paste into the acid solution and water.

Part of the 28-d sample was reserved for scanning electron microscopy energy-dispersive X-ray spectroscopy (SEM-EDS) test. The SEM samples were kept in the original appearance of the fracture surface to see natural microstructure (it affected the quality of picture though). All the rest of the exposed samples were ground with acetone using a pestle and mortar by hand to stop reaction. Fig. 1 shows the experimental procedure.

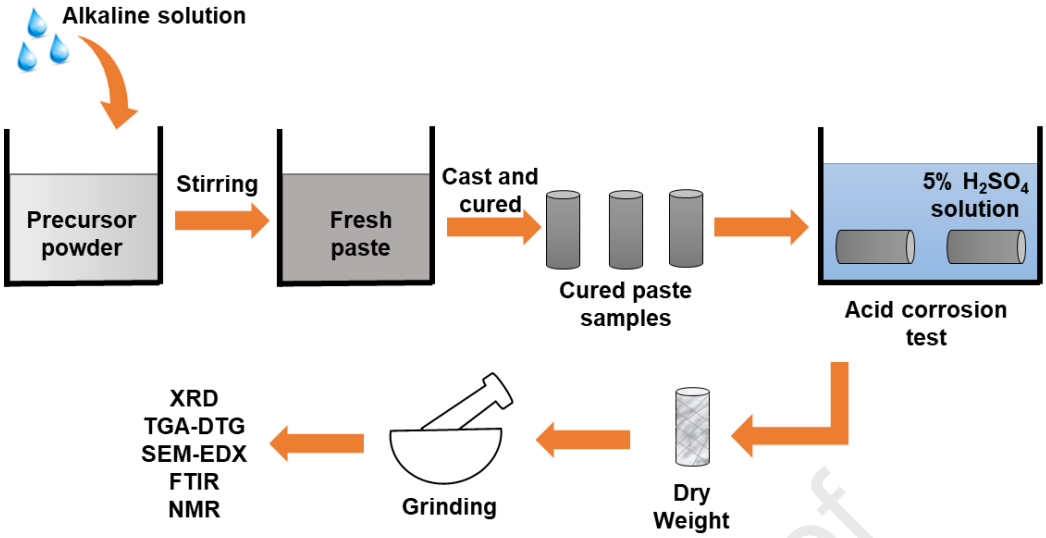

Fig. 1. The experimental procedure.

2.3 Characterisation

The following characterization techniques were used:

- X-ray diffraction (Bruker D8 Advance powder XRD) patterns were collected between 5 and 60° 2θ with a step size of 0.02° 2θ, using Cu Kα radiation with wavelength 1.54 Å, at voltage 40 kV and current 40 mA. Jade 6 software with the powder diffraction file (PDF) database was used to analyse the diffraction patterns.
- Combined thermogravimetric analysis - differential thermogravimetric (TG-DTG) was conducted on TA Instruments Discovery SDT 650. The temperature was increased from room temperature up to 1000 °C at a rate of 10 °C/min in a nitrogen environment. The weight loss information obtained from the TG curve and first derivative (DTG) was used to confirm the type of hydrates and reaction products.
- Fourier transform infrared spectroscopy (FTIR) using Perkin Elmer FTIR-ATR spectrometer in absorbance mode from 4000 to 400 cm^{-1}. Using absorbance values, the spectra were fitted using a baseline correction and deconvoluted in the range of 600 - 1300 cm^{-1} by Origin 9.1 (OriginLab Corporation, USA) with a Gaussian multi-peak fit module.
- Solid-state single pulse ^{27}Al and ^{29}Si magic angle spinning (MAS) NMR spectra were collected on a Bruker 300 MHz Advance III 400WB spectrometer with double air bearing 4 mm MAS probe. Samples were spined at 8 kHz with 1 μs pulse (pi/12) and 1 s relaxation period between scans. The position of peaks was also verified with the

CPMAS spectrum. Repetition delay was 100 s, determined to be sufficient for complete relaxation. Up to 1000 scans were collected. Deconvolution of the ^{29}Si MAS NMR spectra was performed by OriginLab. The minimum possible number of peaks was used to enable an accurate but meaningful interpretation of the spectra.

- SEM-EDS was performed using a Hitachi SU3500 instrument equipped with a 50 mm^2 Oxford Instruments silicon drift detector. Analyses were made at 1000 - 10000 magnification at 5 - 15 kV with lower accelerator energies for imaging with secondary electron returns only and higher accelerator energies for imaging in backscatter mode and the EDS point analyses.

3. Results and discussion

3.1 Visual inspection and mass change

Fig. 2 displays the appearance of the dried NASH sample and C(N)ASH sample before and after 28 days of exposure to sulfuric acid. The surface appearance of unexposed NASH sample was more porous than the C(N)ASH sample. This is partly due to the high reactivity of the aluminosilicate powder for the NASH sample. The rapid coagulation during sample preparation resulted in less compacted paste. On the other hand, it is related to the nature of binding gel formed in each system. It was found that the N-A-S-H gel formed in the fly ash system showed less dense and more porous than the C-(N)-A-S-H gel and C-(A)-S-H gel formed in the slag dominant systems [33]. It agrees with previous findings that C-(N)-A-S-H gel is a space-filling C-(A)-S-H gel which could significantly reduce porosity [34]. After exposure to sulfuric acid solution for 28 days, the NASH sample partially dissolved and had visible cracks around the residual edge of the sample. The exposed C(N)ASH sample suffered severe damage with a completely split which due to the formation of expansive reaction product(s) during acid attack. There was trace amount of calcite formed (as determined by TG-DTG and XRD in the following), which was due to the carbonation on the surface of sample. After exposure to sulfuric acid, the calcite was decomposed completely. Together with the released Ca^{2+} from the dicalcium of C-(N)-A-S-H gels, reactive Ca^{2+} reacts with diffusing SO_4^{2-} ions and forms expansive gypsum, acerated the damaged of the C(N)ASH sample. This was consistent with the previous results that calcium-containing sample showed visible damage [5]. The destruction form of the C(N)ASH sample confirmed the initial failure at the concrete surface, which is the formation of cracks caused surface peeling [5, 22].

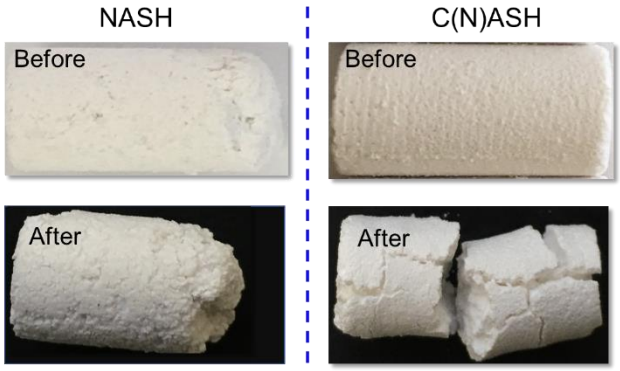

Fig. 2. The appearance of NASH sample and C(N)ASH sample before and after 28 days exposure to sulfuric acid.

Fig. 3 shows the mass changes of the two synthesised NASH sample and C(N)ASH sample after exposure to distilled water and the 5% sulfuric acid solution. Positive value represents a mass gain, and negative value represents a mass loss. In distilled water, a minor mass loss occurred in both the NASH sample and C(N)ASH sample, which was likely due to the leaching of alkali. When exposure to sulfuric acid, it could be observed that the C(N)ASH sample had an evident mass gain over the exposure time, while the NASH sample displayed a mass loss. After 56 days of exposure to sulfuric acid, the C(N)ASH sample had a mass gain of 0.8%, and the NASH sample had a small mass loss of 0.15%. The increased weight of the C(N)ASH sample is related to the formation of reaction products (confirmed in the following sections) and the decreased weight of the NASH sample was due to the dissolution of reaction product. The results are consistent with the above appearance change of the samples. From the results, the distilled water had minor effect on the mass change of samples while the sulfuric acid attack had significant influence on the mass change of samples. This suggests that the synthetic C-(N)-A-S-H and N-A-S-H gels are stable in distilled water while sensitive to sulfuric acid solution. In the following section, the leaching performance of N-A-S-H gel and C-(N)-A-S-H gel in distilled water and sulfuric acid solution could explain this phenomenon.

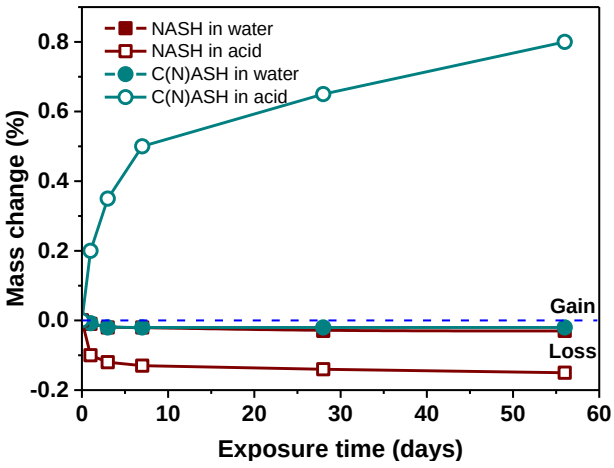

Fig. 3. The mass change (%) of the NASH sample and C(N)ASH sample after exposure to water and 5% sulfuric acid solution.

3.2 Leaching behaviour

Fig. 4 displays the evolution of the pH values of the immersion solutions (i.e. distilled water and the 5% sulfuric acid solutions) with exposure time. As shown in Fig. 4 (a), the initial pH of the distilled water was 6.6, and it increased rapidly to 9 for the NASH sample after 1 day of immersion and remained high thereafter. Similar behavior was observed for the C(N)ASH sample with the pH increased to 12. The increased pH was due to the leaching of hydroxyl ions from samples into the leachates. This took place because of the differential pH between distilled water and samples which were alkaline in nature. The higher pH value of the leachate for the C(N)ASH sample compared to the NASH sample suggests its higher leaching amount of hydroxyl ions (OH^-) from samples.

For the samples immersed in 5% sulfuric acid solution, the pH of the resulted solution for the NASH sample has minor increment from 0.11 to 0.4, while it increased to approximately 2.7 for the C(N)ASH sample. Ions leaching (such as hydroxyl ions) were facilitated by the transfer of acidic ions, i.e. H^+, H_3O^+, and SO_4^{2-}, into the samples, while metal cations (i.e. Ca^{2+}, Al^{3+}, and Na^+) into the acid solution. The consumption of H_3O^+ ions in the sulfuric acid solution of the NASH sample and C(N)ASH sample were 53.2% and 99.75%, respectively, according to acid-base neutralization reaction. The results are consistent with previous findings that the alkali-activated fly ash sample showed lower pH value than the alkali-activated slag after exposure to sulfuric acid solution [5]. As well known the OH^- ions acted as catalyst during alkali-activation process [35]. The greater impact of the C(N)ASH sample on the pH evolution

of both distilled water and sulfuric acid solution was related to its lower consumption of OH^- ions during the formation of reaction products.

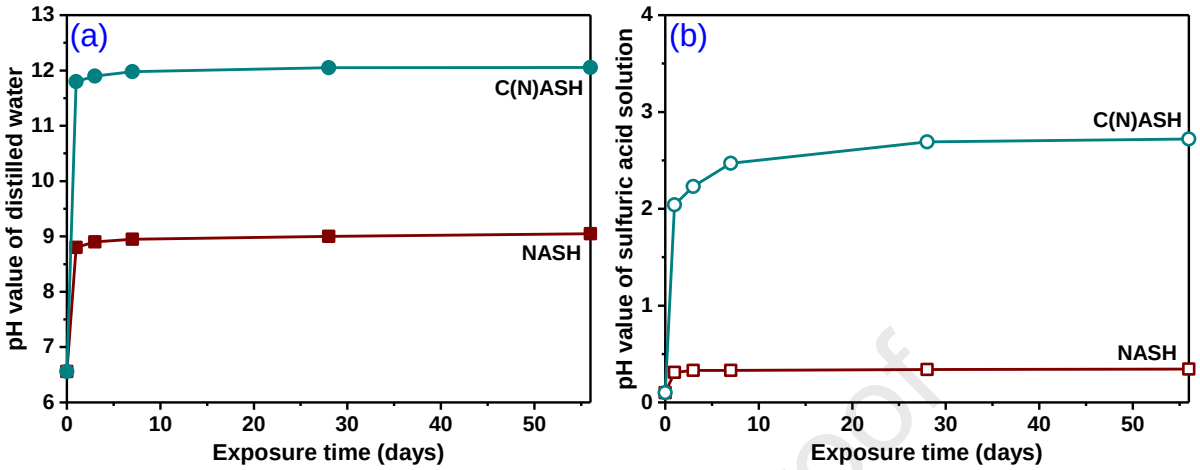

Fig. 4. pH values of the (a) distilled water and (b) 5% sulfuric acid solution after 56 days of immersion of the NASH sample and C(N)ASH sample.

Fig. 5 displays the cumulative concentration of aluminum (Al), calcium (Ca), sodium (Na), and silicon (Si) presented in the distilled water and 5% sulfuric acid solutions during 56-day immersion of NASH sample and C(N)ASH sample. There were no significant quantities of aluminum, calcium, or silicon (< 116, 249, and 145 ppm, respectively) present in the water solutions leached out from any of the NASH sample and C(N)ASH sample. The main element identified in water was sodium, which increased concentration with the exposure time. The cumulative concentration of Na leached out from the NASH sample and C(N)ASH sample was 4886 ppm and 15248 ppm after 56 days exposure to water, respectively. This was not surprising due to the sodium silicate and sodium hydroxide solutions which were used as activators in the mixes. As known, the existing Na in alkali-activated materials included three types, i.e. free Na (the majority), union Na, and compound Na [36]. The free Na existed in the pore solution of the sample and easily diffused into the external environment. Union Na was converted from free Na, existing in an unstable form. The compound Na existed in a stable form in the reaction hydrate, i.e., N-A-S-H gel. The results suggested that more free Na leaching out from the C(N)ASH sample than the NASH sample to distilled water. This result also suggests a possible high efflorescence potential of geopolymer when a small dose of calcium is introduced, and indeed, it has been found by Longhi et al. [37].

For sulfuric acid leachates, a significant amount of aluminum, sodium, and silicon leached out from both the NASH sample and C(N)ASH sample. As shown in Fig. 5 (a), the concentration

of aluminum from the C(N)ASH sample and NASH sample resulted in the highest concentration of 11719 ppm and 38100 ppm, respectively. Higher concentration of Al in the leachate of the NASH sample suggested that the dealumination in the N-A-S-H gel was easier. The calcium content leaching out from the C(N)ASH sample reached the highest value (6830 ppm) on the first day and kept constant thereafter. It is a result of the decalcification of C-(N)-A-S-H gel and the dissolution of other reaction products in the C(N)ASH sample. The concentration of sodium leached from the C(N)ASH sample (41200 ppm) was significantly higher that of the NASH sample (6734 ppm). The bound Na^+ and compound Na^+ are converted back to free Na^+ under acid attack [20], therefore, the Na concentrations were significantly higher in the acid solution leachate than in the water leachate. The difference of sodium concentration in the distilled water and acid solution was regarded to be the amount of bound Na^+ and compound Na^+. The cumulative concentration of silicon leached from the NASH sample and C(N)ASH sample reached 18350 and 8918 ppm, respectively, after 56 days of acid exposure. In view of the above results, the NASH sample showed higher leaching concentrations of Al and Si than the C(N)ASH sample, except for Na.

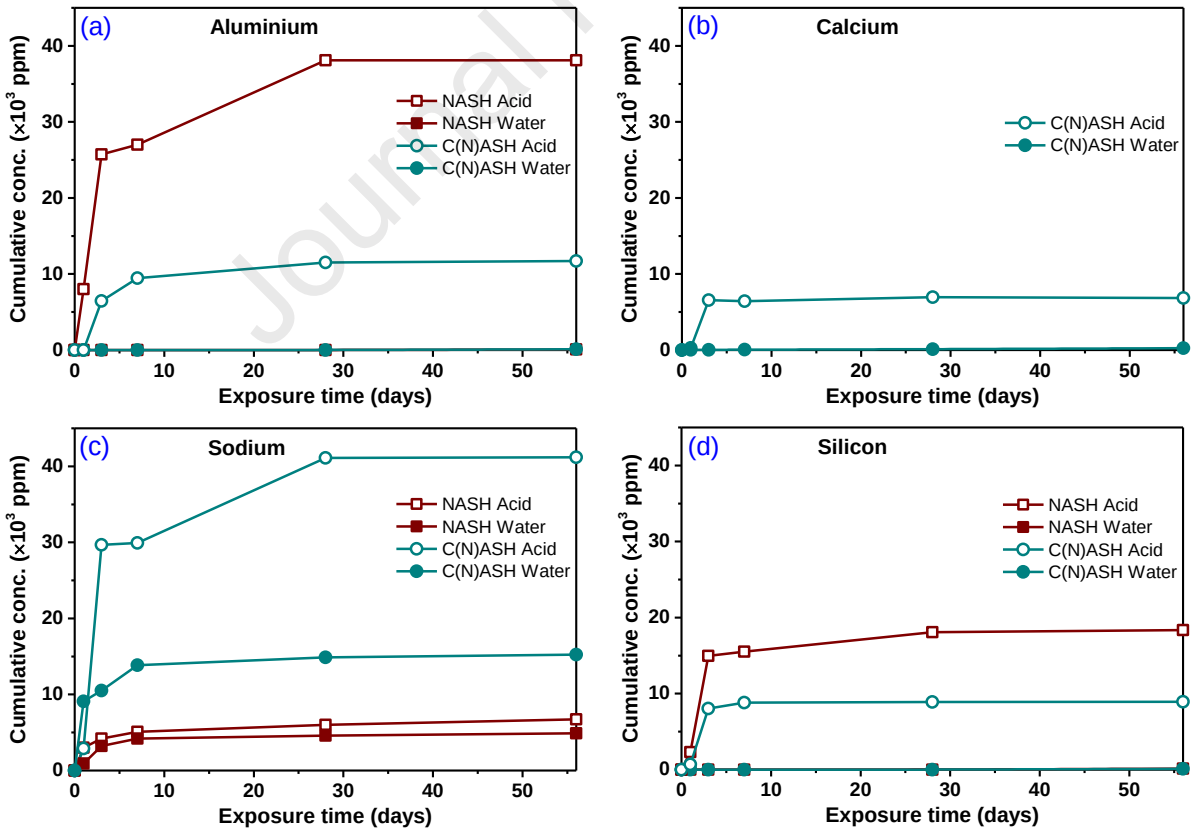

Fig. 5. Cumulative concentrations of aluminium, calcium, sodium, and silicon leached from the NASH sample and C(N)ASH sample exposed to distilled water and 5% sulfuric acid solution for 56 days.

Fig. 6 shows the Si/Al and Na/Al ratios in unexposed NASH sample and C(N)ASH sample and their acid leachates. For the NASH sample, Al was the most easily precipitated element, followed by Na and, lastly Si. The most readily precipitated element in C(N)ASH sample was Na, followed by Al, and finally Si. In view of leaching behaviour, lower concentration of Na was leached out from the NASH sample under sulfuric acid attack. Instead, more Al was leached out from the NASH sample when exposure to acid solution. Hence, Al-O from the framework of N-A-S-H gel was suspensible to hydrogen ions attack. It means the destroy of N-A-S-H gel under acid conditions is due to dealumination from the gel framework, while the destroy of C-(N)-A-S-H gel under acid conditions is due to the continuous leaching of Na, together with the continuous loss of Al (dealumination). This is different from the previous mechanism that for the C-S-H gels that formed in OPC system, which the sulphuric acid leads to the decalcification and finally destroy of matrix.

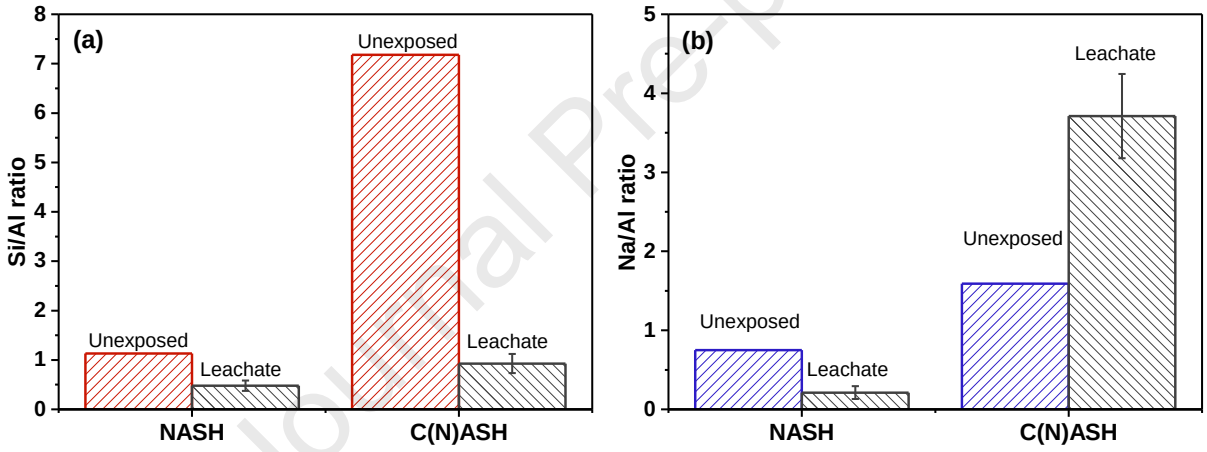

Fig. 6. The ratios of (a) Si/Al and (b) Na/Al in the unexposed NASH sample and C(N)ASH sample and their acid leachates.

3.3 X-ray diffraction (XRD) analysis

Fig. 7 shows the XRD results for the NASH sample and C(N)ASH sample before and after 28 days of sulfuric acid exposure. As shown in Fig. 7 (a), a broad featureless hump was visible between 20° and 35° 2θ for the NASH sample, confirmed the formation of amorphous reaction products (i.e. N-A-S-H gel) as discussed above [33]. The minor crystalline peaks observed in the NASH sample were attributed to the phases like paragonite ($NaAl_2(AlSi_3)O_{10}(OH)_2$, PDF # 24-1047) and albite ($NaAlSi_3O_8$, PDF # 80-1094). After sulfuric acid exposure, the broad peak at the NASH sample shifted to around 22° 2θ, suggesting the breakage of the N-A-S-H gel [20]. This result suggested that the N-A-S-H gel was vulnerable to sulfuric acid attack.

Paragonite and albite were on longer present in the exposed NASH sample. This was different to the crystalline phases found in alkali-activated fly ash which was invulnerable to sulfuric acid attack [5]. The peaks attributed to tamarugite ($NaAl(SO_4)_2 \cdot 6H_2O$, PDF # 71-2385) was identified in the exposed NASH sample. This suggests that the decomposition of N-A-S-H gel leads to the precipitation of Na and Al in the leachates.

As shown in Fig. 7 (b), the XRD pattern of the C(N)ASH sample exhibits a broad feature centered at approximately 29° 2θ, characteristic of a disordered reaction product consistent with that formed in AAMs derived from slag [32]. This phase was assigned to a poorly crystalline C-(A)-S-H phase displaying some structural similarity with calcium aluminum silicate (CAS, PDF # 23-0105). Calcite ($CaCO_3$, PDF # 72-1937 and PDF # 41-1475) was formed at the similar reflection angel with CAS which was formed during preparation process. Pectolite ($NaCa_2HSi_3O_9$, PDF # 33-1223), wollastonite ($CaSiO_3$, PDF # 84-0654) and calcium aluminite silicate ($Ca_3Al_6Si_3O_{16}$, PDF # 47-0162) were also identified in the unexposed C(N)ASH sample. After exposure to sulfuric acid for 28 days, the exposed C(N)ASH sample demonstrated the presence of gypsum ($CaSO_4 \cdot 2H_2O$, PDF#33-0311). The trace of amorphous hump shifted to around 22° 2θ and decreased in the intensity, which was considered as the distinguishing feature of residual C-(A)-S-H gel. The crystalline phases identified in unexposed C(N)ASH sample was no longer present. There was no ettringite identified in the XRD pattern of the exposed C(N)ASH sample. This is due to the formation of gypsum is favored than ettringite when calcium availability was enough [38]. The findings explain the different appearance changes of the NASH sample and C(N)ASH sample when exposed to acid, as discussed above.

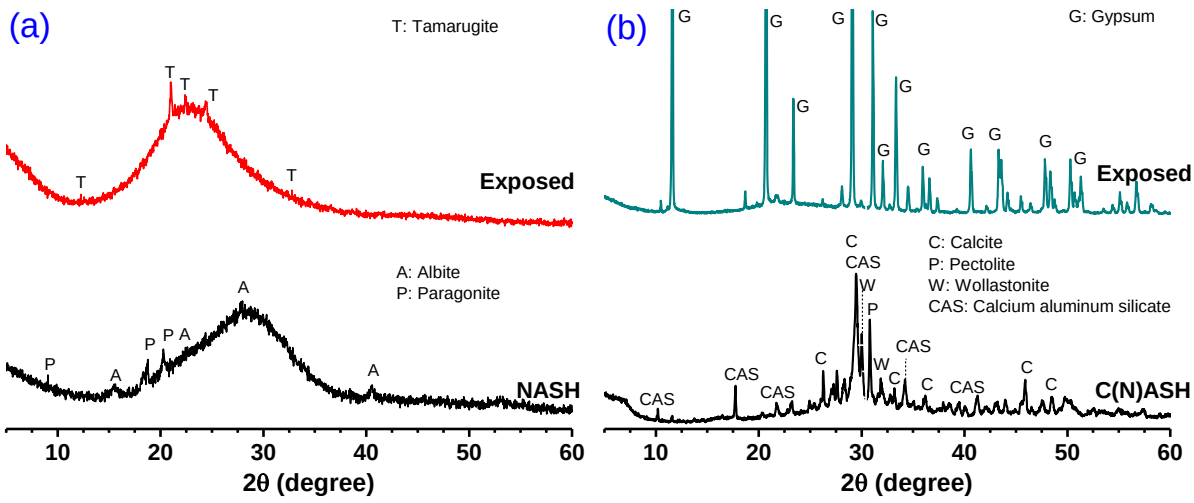

Fig. 7. X-ray diffractions of the (a) NASH sample and (b) C(N)ASH sample before and after 28 days sulfuric acid attack.

3.4 Thermogravimetric-differential thermogravimetric (TG-DTG) analysis

Fig. 8 displays the mass change at high temperatures of the NASH sample and C(N)ASH sample before and after exposure to sulfuric acid attack. The unexposed and exposed NASH samples showed final mass loss of 27.8% and 29.7%, respectively. For the unexposed NASH sample, the mass loss peak in the DTG curves centred at 71 °C, which was due to the removal of free water [32]. The larger shoulder at around 105 °C for the unexposed NASH sample was attributed to the dehydration of gel product (i.e. N-A-S-H gel), which continued to around 300 °C [39]. A small mass loss peak was observed at 255 °C which was associated with the loss of tightly physically bound water in albite and paragonite, identified in the XRD patterns [32, 40]. After exposed to acid attack, the mass loss peak due to the removal of free water shifted to a higher temperature at around 78 °C. The reduced intensity of dehydration peak at around 105 °C suggested that reduced amount of bound water of N-A-S-H gel when exposed to sulfuric acid. Another mass loss happened in the range of 416-617 °C, which was due to the dehydration of reaction product (tamarugite) [41-43].

The C(N)ASH sample before and after exposure to sulfuric acid attack showed the final mass loss of 12.5% and 17.9%, respectively. The mass loss of the unexposed C(N)ASH sample continued to around 650 °C, while the mass loss of the exposed C(N)ASH sample happened predominately before 300 °C. The mass loss happened in the range of 30 °C to 680 °C in the DTG curve of the unexposed C(N)ASH sample which was related to the removal of free water and the dehydration of C-(N)-A-S-H gel [43]. The small peak at 676 and 680 °C suggested the decomposition of calcite [44, 45]. The mass loss peak of the exposed C(N)ASH sample before 100 °C was the removal of free water and/or loosely bound moisture which was not removed during preparation of the powdered sample [5]. The mass loss peak at the range of approximately 90 and 150 °C were believed to be due to the dehydration of gypsum, as shown in Eq. 2 and Eq. 3 [46-49].

The weight loss due to the decomposition of gypsum can be used to calculate the amount of gypsum present in the exposed samples, using the molecular mass of gypsum and water as shown in Eq. 2 and Eq. 3 [43]. Considering the contribution of water loss from the C-(N)-A-S-H gel (it can be obtained from the deconvoluted peaks of the DTG curves of the exposed

C(N)ASH sample), the amount of calculated $CaSO_4 \cdot 2H_2O$ accounted for around 60 wt.% of the exposed sample, see details in Appendix I.

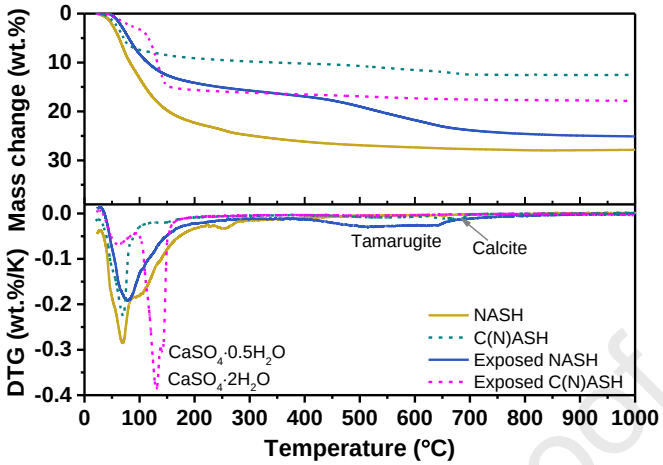

Fig. 8. Mass change and differential mass change (DTG) of the NASH sample and C(N)ASH sample before and after 28 days of sulfuric acid attack.

$$CaSO_4 \cdot 2H_2O \xrightarrow{90\text{-}170\ ℃} CaSO_4 \cdot 0.5H_2O + 1.5H_2O \quad \text{Eq. 2}$$

172 g/mol 145 g/mol 27 g/mol

$$CaSO_4 \cdot 0.5H_2O \xrightarrow{115\text{-}150\ ℃} CaSO_4 + 0.5H_2O \quad \text{Eq. 3}$$

145 g/mol 136 g/mol 9 g/mol

3.5 Fourier transform infrared spectroscopy (FTIR) analysis

Fig. 9 presents the FTIR spectra for the precursors and the NASH sample and C(N)ASH sample before and after exposure to sulfuric acid attack. In the spectrum of the precursor for the NASH sample, an intense peak was observed at approximately 1072 cm^{-1}, which was assigned to asymmetric stretching vibrations of Si-O-T bonds, where T = Si or Al in tetrahedral coordination [50]. The band at approximately 781 cm^{-1} that was assigned to bending vibrations of Al-O bonds in AlO_6 octahedra [51]. In the spectrum of the precursor for the C(N)ASH sample, a broad band was observed at 910 cm^{-1}, and a shoulder could also be observed at 993 cm^{-1}. These bands were attributed to the stretching vibrations of Si-O-T bonds due to a highly depolymerized silica network and consistent with that observed in slag [32, 52]. A sharp shoulder at 841 cm^{-1} was likely due to the presence of HCO_3^- formed during sample preparation [32]. The small featural bands centered at 696 and 460 cm^{-1} were attributed to symmetrical stretching and bending of Si-O-T bonds, respectively [32].

The alkali activation process in the NASH sample is observed by the shifting of the main peak from 1072 cm^{-1} to 972 cm^{-1}. This change was due to the decrease of tetrahedral Si sites, replaced by the tetrahedral Al during the formation of N-A-S-H gel [20]. The small band observed at approximately 1647 cm^{-1} for each sample was assigned to H-O-H bending mode [5]. The broad band at the range of about 3700-2700 cm^{-1} was attributed to the presence of free and chemically bound water due to the activation process. For C(N)ASH sample, alkali-activation produced a broad intense band at approximately 955 cm^{-1}, attributed to asymmetric stretching vibrations of Si-O-T bonds in the chain structure of C-(N)-A-S-H gel [53]. The broad band at 1417 cm^{-1} was attributed to the asymmetric stretching of O-C-O bonds in CO_3^{2-}.

FTIR data for the NASH sample after exposure to acid attack exhibited a movement of the main peak to a higher wavenumber from 972 cm^{-1} to 1060 cm^{-1}. This change was related to the decomposition of N-A-S-H gel under acid attack. Two more intensive peaks at 945 cm^{-1} and 797 cm^{-1} in the corroded NASH sample were recognized as the residual N-A-S-H gel. Sulfuric acid attack caused a significant change on the FTIR spectrum of the exposed C(N)ASH sample. The main band was centered at approximately 1100 cm^{-1}, and two intensive peaks formed at 667 cm^{-1} and 600 cm^{-1}. These changes indicated the decomposition of C-(N)-A-S-H gel and the formation of corrosion products, mainly gypsum.

The overlapping bonds are identified in the FTIR spectra by deconvolution of the main band, which are summarized in Table 2. For NASH sample, the bands at 1050 cm^{-1} and 987 cm^{-1} were assigned to the asymmetric stretching vibration (σ_{as}) of Si-O-T bond, and 947 cm^{-1} to asymmetric stretching vibration of non-bridging oxygen sites (i.e. Si-O-Na). The bands at 853 cm^{-1} and 712 cm^{-1} were assigned to the bending vibration (δ) of Si-OH bond and Si-O-Al^{IV} bond, respectively. After exposed to sulfuric acid attack, new bands appeared at 1214 cm^{-1} and 1118 cm^{-1} were assigned to the asymmetric stretching vibration of S-O bond in SO_4^{2-}, accounting for around 36 % [54]. High polymerized Si-O bonds at 1071 cm^{-1} and 1034 cm^{-1} were accounted for 51% since the dealumination of the N-A-S-H gel leaving a silica-rich gel. There was no Si-O-Al^{IV} identified in the exposed NASH sample. The results confirmed that acid attack resulted in the dealumination of N-A-S-H gel and breakdown of Si-O-Na bond. Al was easier leaching out from N-A-S-H gel than Na and the delamination resulted the destroy of N-A-S-H gel under acid attack.

Compared to the NASH sample, the Al-substitution in the C-(N)-A-S-H gel of the C(N)ASH sample could be deconvoluted out as Si-O-Al bond at 1023 cm^{-1}. The Si-O-Na bond in the C-

(N)-A-S-H gel accounted for around 2%, much less than 19% in the N-A-S-H gel. This was likely related to the different action mechanism of alkali in the N-A-S-H gel and C-(N)-A-S-H gel, while Na incorporated into silicate chains in the N-A-S-H gel but acted as charge balance in the C-(N)-A-S-H gel at Al-substitution site. After exposed to sulfuric acid attack, the Si-O-Na bond in the exposed C-(N)-A-S-H gel could still be identified. The results suggested that acid attack caused the dealumination of the C-(N)-A-S-H gel along with leaching of alkali but had minor effect on the Si-O-Na bond in the C-(N)-A-S-H gel.

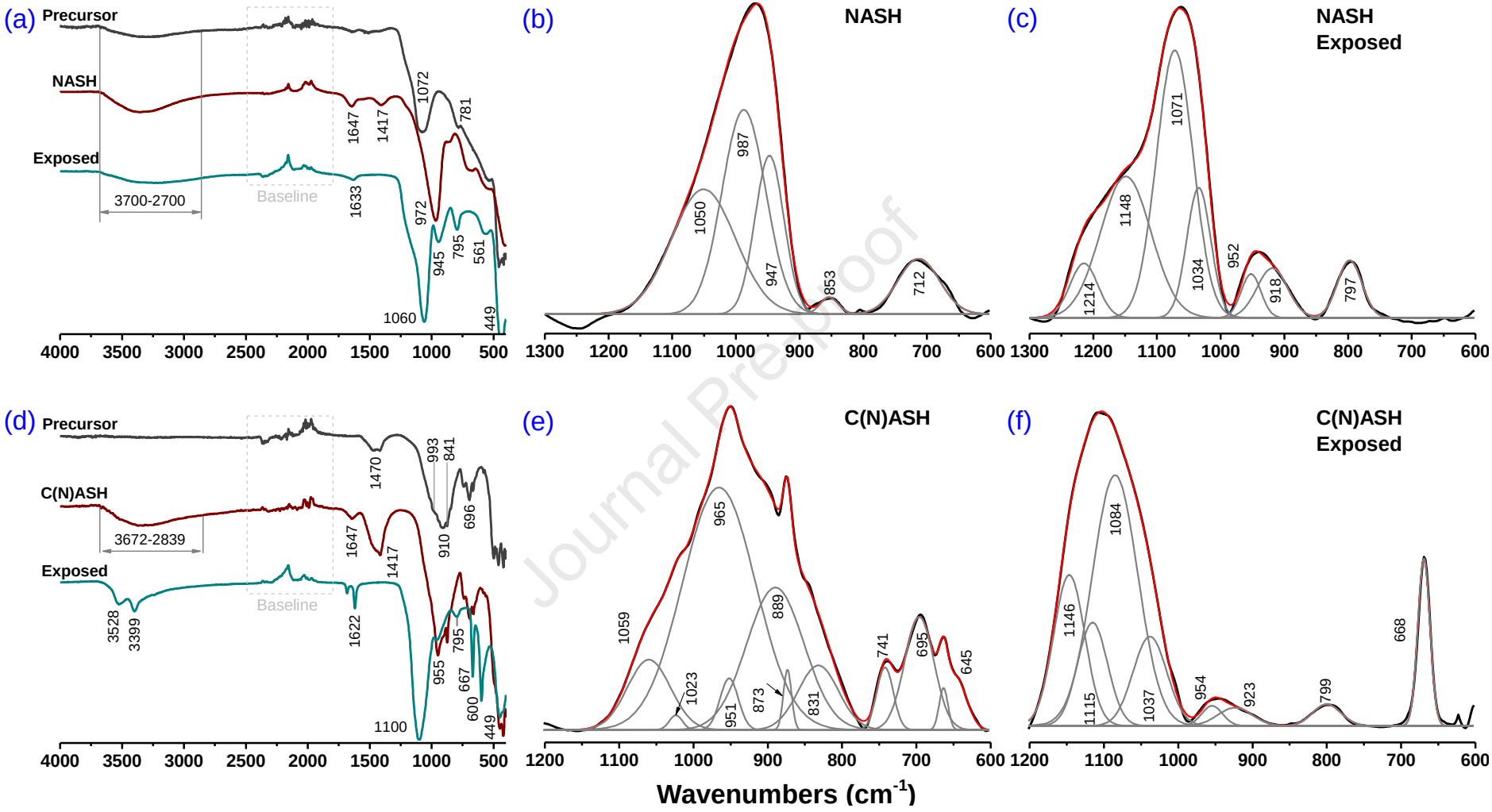

418

419 Fig. 9. FTIR spectra (absorbance) and deconvoluted spectra of the NASH and C(N)ASH samples before and after exposure to sulfuric acid.

Table 2 Summary of bands in the deconvoluted FTIR spectrum of Si-O-T bands for the NASH and C(N)ASH samples before and after exposed to acid attack in the range of 1300 cm^{-1} ~ 600 cm^{-1}. Asymmetric stretching vibration (σ_{as}), symmetric stretching vibration (σ_s) and bending vibration (δ). * means bands with trace occupation.

	Position (cm^{-1})	Assignment	Account (Relative area %)	Ref.
NASH	1050	σ_{as} Si-O, Q^3+ Q^4	33	[50, 55]
	987	σ_{as} Si-O, Q^2	37	[55]
	947	σ_{as} Si-O-Na	19	[51]
	853	δ Si-O	1	[51]
	712	δ Si-O-Al^{IV}	10	[51]
Exposed NASH	1214	σ_{as} SO_4^{2-}	8	[54]
	1118	σ_{as} SO_4^{2-}	28	[54]
	1071	σ_{as} Si-O, Q^4, silica gel	39	[54]
	1034	σ_{as} Si-O, Q^3, silica gel	12	[55]
	952	σ_{as} Si-O-Na	3	[55]
	918	σ_{as} Si-O	6	[51]
	797	δ Si-O	6	[51]
C(N)ASH	1059	σ_{as} Si-O, Q^3+ Q^4	8	[55]
	1023*	σ_{as} Si-O-Al	0.5	[55]
	965	σ_{as} Si-O, Q^2	46	[55]
	951*	σ_{as} Si-O-Na	2	[55]
	889	δ Si-O	21	[51]
	873*	σ_{as} C-O	1	[51]
	831	σ_s Si-O, C-S-H	7	[56]
	741	δ Si-O-T, precursor	3	[51]
	695	δ Si-O-T, precursor	9	[51]
	645	δ Si-O-T, precursor	3	[51]
Exposed C(N)ASH	1146	σ_{as} SO_4^{2-}, gypsum	18	[54]
	1115	σ_{as} SO_4^{2-}, gypsum	12	[54]
	1084	σ_{as} Si-O, Q^4, silica gel	44	[55]
	1037	σ_{as} Si-O, Q^3, silica gel	12	[55]
	954	σ_{as} Si-O-Na	2	[55]
	923	σ_{as} Si-O	2	[55]
	799	δ Si-O	2	[51]
	668	σ_{as} SO_4^{2-}, gypsum	8	[54]

3.6 Scanning electron microscopy (SEM) and energy dispersive X-ray (EDX) analysis

Fig. 10 shows the SEM images of NASH sample and C(N)ASH sample before and after exposure to sulfuric acid attack. The fracture section of the unexposed NASH sample showed a homogeneous but granular surface. After acid attack, the microcracks generated inside the paste matrix. This was due to the leaching of aluminium and sodium from the paste of NASH sample. The unexposed C(N)ASH sample showed a denser microstructure than the NASH sample. After exposed to acid attack, it was clear to see the formation of column-like gypsum

grains in the exposed C(N)ASH sample. The coarse gypsum grains forming in a dense matrix can result in high stress and lead to loosening of the C(N)ASH matrix, and further cracking of the samples (as shown in Fig. 2).

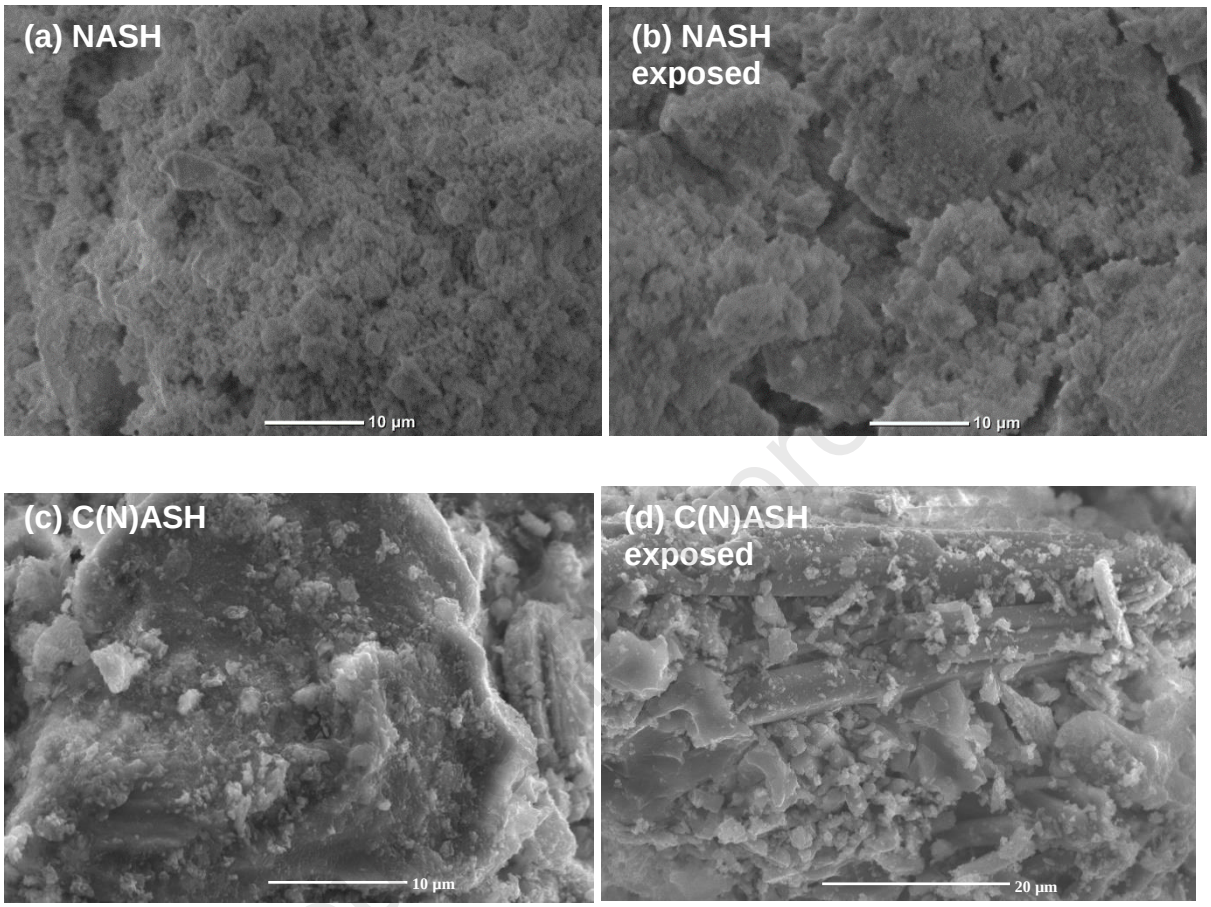

Fig. 10. SEM images of the NASH and C(N)ASH samples before and after exposure to sulfuric acid.

Fig. 11 shows the summary of atomic ratios of Na/Al versus Si/Al for the NASH sample before and after unexposed to acid attack. The elemental composition of unexposed NASH sample displayed a broad range of values within the region $1.0 \leq Si/Al \leq 4.5$ and $0.5 \leq Na/Al \leq 2.0$, which was comparable with that of alkali-activated fly ash [14]. After exposed to acid for 28 days, the exposed NASH sample exhibited a range of values clustered around two distinct regions: one with the cation ratios of $3.5 \leq Si/Al \leq 5.2$ and $3.5 \leq Na/Al \leq 6$, and another with the cation ratios of $4 \leq Si/Al \leq 5.2$ with free Na. This suggested that sulfuric acid attack resulted in the residual N-A-S-H gel exhibiting a high Si/Al ratio due to the dealumination. Meanwhile, sodium leaching out from the N-A-S-H gel resulting in Na/Al ratio near 0.

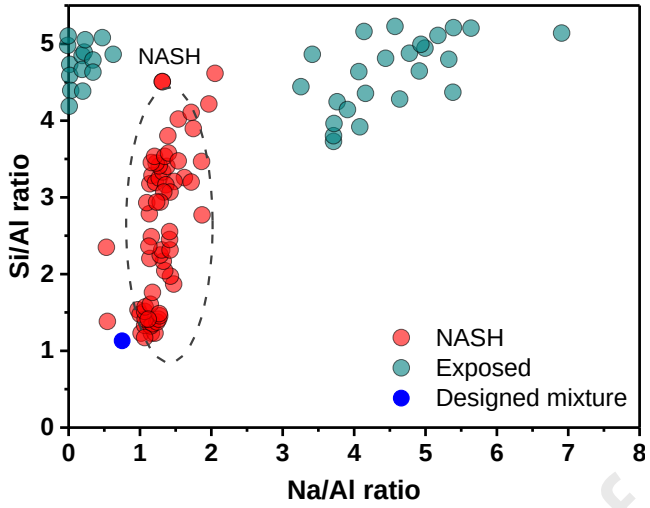

446

447 Fig. 11. Atomic ratios Na/Al versus Si/Al for the unexposed and exposed regions of the NASH sample
448 as marked, determined by EDX analysis. A random selection of points evenly distributed across a
449 representative 1000 μm × 1000 μm section of the sample were used for analysis. The approximate
450 region defined for N-A-S-H refers to [32].

451 Fig. 12 shows the summary of atomic ratios Ca/Si versus Al/Si for projection of material
452 chemistry of the unexposed and exposed C(N)ASH samples. The chemistry of the unexposed
453 C(N)ASH sample lied within the region commonly associated with a C-(N)-A-S-H gel of 0.79
454 ≤ Ca/Si ≤ 1.86 and 0.11 ≤ Al/Si ≤ 0.28. After exposed to sulfuric acid attack for 28 days, the
455 chemistry of the exposed C(N)ASH sample showed two regions: one with the cation ratios of
456 0 ≤ Al/Si ≤ 0.1 and 0 ≤ Ca/Si ≤ 2, and another which exhibited cation ratios of Al/Si = 0 and 0
457 ≤ Ca/Si ≤ 15. The very high Ca/Si is due to the formation of gypsum as EDS analysis may
458 bring in a region of elements into counting. It means the destroy of C-(N)-A-S-H gel under
459 acid conditions related to both dealumination and decalcification.

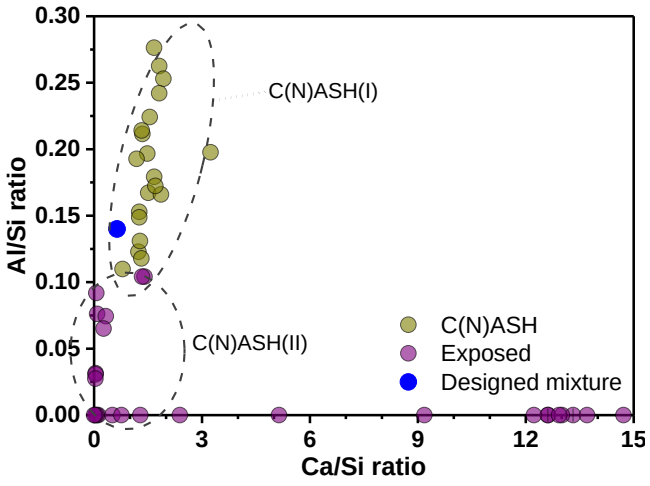

460

461 Fig. 12. Atomic ratios Ca/Si versus Al/Si for the unexposed and exposed regions of the C(N)ASH
462 sample as marked, determined by EDX analysis. A random selection of points evenly distributed across

a representative 1000 μm × 1000 μm section of the sample were used for analysis. Approximate regions of C-(N)-A-S-H are determined from [32].

3.7 Solid-state MAS NMR spectroscopy analysis

3.7.1 ^{27}Al MAS NMR spectroscopy

Fig. 13 shows the ^{27}Al MAS NMR spectra of the NASH sample and C(N)ASH sample before and after exposure to acid attack. From Fig. 13 (a), the unexposed NASH sample consisted of one main resonance centered at 55 ppm, which was assigned to aluminum in tetrahedral (Al^{IV}) coordination [32]. The Al^{IV} was assigned in a q^4 (i.e. q^4 = Si is in tetrahedral coordination and bonded to 4 other tetrahedral atoms) environment within a highly polymerized N-A-S-H gel framework [20, 57]. A low-intensity resonance at δ_{obs} = 4 ppm was attributed to octahedral (Al^{VI}) coordination in the unreacted precursor [32]. The spectra of precursor powder was typical of those commonly observed for aluminosilicate glasses, displaying three broad peaks which are assigned to tetrahedral (Al^{IV}), pentahedral (Al^{V}), and octahedral (Al^{VI}) aluminum [32]. During the alkali-activation process, Al^{V} and Al^{VI} within precursor powder dissolved and reacted to form Al^{IV} species [57]. After exposure to acid attack for 28 days, the exposed NASH sample showed two narrow resonances centered at -1 ppm and -4.6 ppm, respectively, which were both assigned to Al^{VI} in a well-defined octahedral coordination [32]. This was consistent with greater stability of Al^{VI} species under acidic conditions when compared to Al^{IV} and Al^{V} species [20]. In view of the above results, the dealumination and sodium removal from the N-A-S-H gel resulted in the decomposition of the solid phase in the NASH sample.

The spectra of the unexposed C(N)ASH sample displayed a broad resonance spanning from 20 ppm to 80 ppm and centered at approximately 58 ppm, which was assigned to tetrahedral (Al^{IV}) coordination in geopolymer binder [32]. The broad contribution of q^4(4Si) species indicated a significant crosslinking of C-(N)-A-S-H gel [32]. The spectra of the exposed C(N)ASH sample showed a narrow resonance at approximately 0 ppm which was assigned to Al^{VI} in well-defined octahedral coordination, as well remained a low-intensity broad resonance spanning from 40 ppm to 60 ppm as shown in Fig. 13 (b). The formation of aluminum sulfate was contributed to the resonance at around 0 ppm. The resonance at 50 ppm was assigned to the tetrahedral (Al^{IV}) coordination in the residual C-(N)-A-S-H gel.

The broad resonance of ^{27}Al MAS NMR spectra of the NASH sample and C(N)ASH sample before exposure to acid attack suggested that Al predominantly existed in a distorted tetrahedral environment q^4(4Si) in both N-A-S-H gel and C-(N)-A-S-H gel. However, the resonance of Al

in the C-(N)-A-S-H gel showed slightly wider than that in the N-A-S-H gel. It means more complicated Al environment in the C-(N)-A-S-H gel. After exposure to sulfuric acid, the Al environment in the N-A-S-H gel was easily attacked and combined Al was converted into movable ions. There was no remaining undamaged Al environment and the Al in the residual sample was in an active state. It could be seen that a part of original Al environment in the C-(N)-A-S-H gel was undamaged by acid attack, and less active Al was identified than N-A-S-H gel. When combined with the appearance change, it was found that, whereas the appearance of the NASH sample had not altered significantly, the N-A-S-H gel had been completely destroyed. Even though the C(N)ASH sample had cracks, a portion of the C-(N)-A-S-H gel persisted.

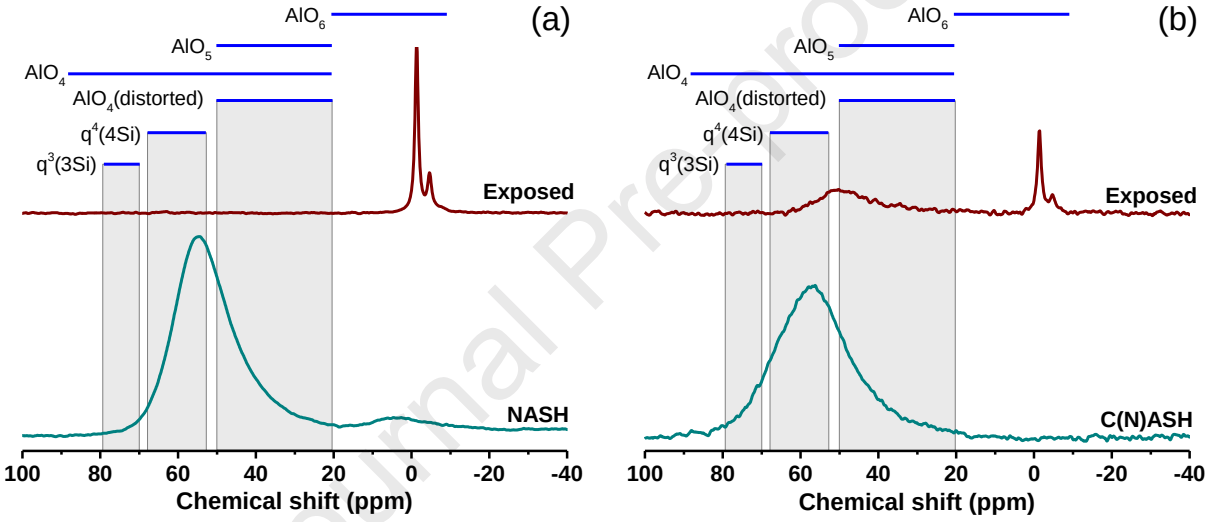

Fig. 13. ^{27}Al MAS NMR data of the NASH sample and C(N)ASH sample before and after exposure to sulfuric acid attack.

3.7.2 ^{29}Si MAS NMR spectroscopy

The ^{29}Si MAS NMR spectra and deconvoluted peaks for the NASH sample and C(N)ASH sample before and after exposed to sulfuric acid are presented in Fig. 14 and Fig. 15. According to [58], Si sites were generally identified using the notation of the type $Q^n(mAl)$ with $0 \leq m \leq n \leq 4$, where Si in tetrahedral coordination (represented by Q) was bonded to n other tetrahedral units (m is the number of Al) via oxygen bridges. The summary of the deconvolution peaks is shown in Table 3. As shown in Fig. 14 (a), the ^{29}Si MAS NMR spectra of the unexposed NASH sample was deconvoluted into eight peaks which indicating Si environments attributed to $Q^4(0Al)$, $Q^4(1Al)$, $Q^4(2Al)$, $Q^4(3Al)$, Q^3, Q^2, $Q^2(1Al)$ and Q^0, in agreement with other studies [2, 18, 32]. The Q^0 resonance might be attributed to dissolved precursors or monomer silicate structures from remnant soluble silicate that has not react [20]. The Q^3 and Q^2 sites resonate

519 exists in this study. This is contradictory with the results of N-A-S-H gel derived from
520 metakaolin [20]. There is no Q^1 site in the spectra of the unexposed NASH sample. The results
521 indicate that the framework of N-A-S-H is highly polymerised [18]. After exposure to acid
522 attack, the deconvoluted peaks of the exposed NASH sample are contributed to Q^3(1Al),
523 Q^4(3Al), Q^4(2Al), Q^4(1Al) and Q^4(0Al) sites. There is no Q^2, Q^1, and Q^0 sites remained in the
524 residual gel. It should be noted that there is no Al in tetrahedral coordination from ^{27}Al MAS
525 NMR data (presented above) in the exposed NASH sample. This is because that part of the
526 [AlO_4] tetrahedrons detach from Si-O-Al bond under acid attack and leach out from the
527 framework of N-A-S-H gel. And part of the [AlO_4] tetrahedrons transfer to octahedrons that
528 Al in six coordination and incorporate into the Si-O-Al bond in the residual gels. This increases
529 the polymerization of residual gels.

530 Engelhardt's formula (Eq. 4) was used to calculate the molar Si/Al ratio of the N-A-S-H gel
531 before and after exposure to sulfuric acid in the NASH sample [20]. The Si/Al ratio of the
532 unexposed NASH sample is 1.9 while increased to 2.3 after exposure to sulfuric acid. The
533 results show that the dealumination of N-A-S-H gel is along with a higher Si/Al ratio in residual
534 gel and higher polymerization.

$$\frac{\mathrm{Si}}{\mathrm{Al}} = \frac{\sum_{m=1}^{4} I_{\mathrm{A}_{\mathrm{Q}^4(m\mathrm{Al})}}}{\sum_{m=1}^{4} 0.25 \times m \times I_{\mathrm{A}_{\mathrm{Q}^4(m\mathrm{Al})}}} \qquad \text{Eq. 4}$$

535 Where, $I_{\mathrm{A}_{\mathrm{Q}^4(m\mathrm{Al})}}$ is the normalized relative integral areas of each deconvoluted Q^4(mAl) peaks
536 as shown in Table 3.

537 The ^{29}Si MAS NMR spectra and deconvoluted peaks of the unexposed C(N)ASH sample and
538 exposed C(N)ASH sample are presented in Fig. 15.

$$\frac{\mathrm{Si}}{\mathrm{Al}} = \frac{\sum_{m=1}^{4} \mathrm{I}_{\mathrm{A}_{\mathrm{Q}^4(mAl)}}}{\sum_{m=1}^{4} 0.25 \times m \times I_{\mathrm{A}_{\mathrm{Q}^4(mAl)}}} \qquad \text{Eq. 4}$$

539 Where, $I_{\mathrm{A}_{\mathrm{Q}^4(m\mathrm{Al})}}$ is the normalized relative integral areas of each deconvoluted Q^4(mAl) peaks
540 as shown in Table 3. Where, $I_{\mathrm{A}_{\mathrm{Q}^4(mAl)}}$ is the normalized relative integral areas of each
541 deconvoluted Q^4(mAl) peaks as shown in Table 3. The ^{29}Si MAS NMR spectra of the
542 unexposed C(N)ASH sample displays a relative narrowing resonance spanning from -70 to -
543 100 ppm, which were deconvoluted into peaks at -98, -95, -92, -87, -84, -80, and -76 ppm,

attributed to Q^4(3Al), Q^4(4Al), Q^3, Q^3(1Al), Q^2, Q^2(1Al), Q^1, and Q^0, respectively. The reduced width of resonance and the increased intensity of Q^2, Q^1, and Q^0 sites suggested that the C-(N)-A-S-H gel showed higher order than the N-A-S-H gel (in agreement with XRD analysis). The chemical shifting to lower field indicates the change of Si environments due to Q^4(mAl) loss in the exposed C(N)ASH sample. This also confirms the dealumination mechanism of C-(N)-A-S-H gel as discussed above.

According to [18], the MCL and molar Si/Al ratio of the non-crosslinked and crosslinked C-(N)-A-S-H gel can be determined based on the following equations (Eq. 5 to Eq. 8):

$$MCL_{[NC]}=\frac{2I_A[Q^1+Q^2+\frac{3}{2}Q^2(1Al)]}{I_A(Q^1)} \quad \text{Eq. 5}$$

$$\frac{Si}{Al}_{[NC]}=\frac{2I_A[Q^1+Q^2+Q^2(1Al)]}{I_A[Q^2(1Al)]} \quad \text{Eq. 6}$$

$$MCL_{[C]}=\frac{4I_A[Q^1+Q^2+Q^2(1Al)+Q^3+2Q^3(1Al)]}{I_A(Q^1)} \quad \text{Eq. 7}$$

$$\frac{Si}{Al}_{[C]}=\frac{I_A[Q^3(1Al)]}{I_A[Q^1+Q^2+Q^2(1Al)+Q^3+Q^3(1Al)]} \quad \text{Eq. 8}$$

where [C] denotes crosslinked C-(N)-A-S-H structures and [NC] denotes non-crosslinked C-(N)-A-S-H structures.

In the unexposed C(N)ASH sample, the MCL and Si/Al ratio of non-crosslinked C-(N)-A-S-H gel are 9.0 and 5.7, respectively. The synthetic C-(N)-A-S-H gel displays a similar MCL and Si/Al ratios as the alkali-activated fly ash/slag pastes, which showed a range of 6.43-9.76 for MCL and corresponding Si/Al ratio of 6.35-4.74 [59]. After exposed to sulfuric acid, the MCL reduces to 6.7 and the Si/Al reduces to 3.3. The reduced MCL indicates the shorten of the framework in the non-crosslinked C-(N)-A-S-H gel after acid attack which is due to dealumination. The declined Si/Al ratio is due to the change of the coordination of Al from four to six, which is consistent with the ^{27}Al MAS NMR results. The MCL and Si/Al ratio of the crosslinked C-(N)-A-S-H gel increase from 22 to 26 and from 0.13 to 0.45, respectively, after exposed to sulfuric acid solution. The acid attack caused increment of crosslinked C-(N)-A-S-H gel with minor changes in the chain length. However, the exposed C-(N)-A-S-H gel shows a similar framework like N-A-S-H gel, which could be seen from the high intensity of Q^4(mAl) resonance, as shown in Fig. 15 (b). Thus, the Si/Al ratio calculated based on Engelhardt's formula (Eq. 4) is 3.8, which is higher than that of the exposed N-A-S-H gel. The results confirm that the decalcification in C-(N)-A-S-H gel leads to a destruction of the orderly

layered structure. Further exploration on the acid corrosion mechanism of the C-(N)-A-S-H gel could focus on the effect of Ca/Si ratio in this type of gel.

The N-A-S-H gel shows higher polymerization (higher MCL) and lower Si/Al than the C-(N)-A-S-H gel. After exposure to sulfuric acid, the exposed N-A-S-H gel showed increased polymerization and increased Si/Al ratio due to the dealumination, while the C-(N)-A-S-H gel increased crosslinking with reduced Si/Al ratio due to decalcification. The change of Si/Al ratio of the C-(N)-A-S-H gel is inconsistent with that from SEM-EDX results. This suggests that an elemental mapping characterization analysis on the bulk area of alkali-activated materials is hard to explain the intrinsic change of their reaction products. Overall, it is confirmed that the silicon chains in N-A-S-H gel and C-(N)-A-S-H gel tend to form highly crosslinked silica framework after sulfuric acid.

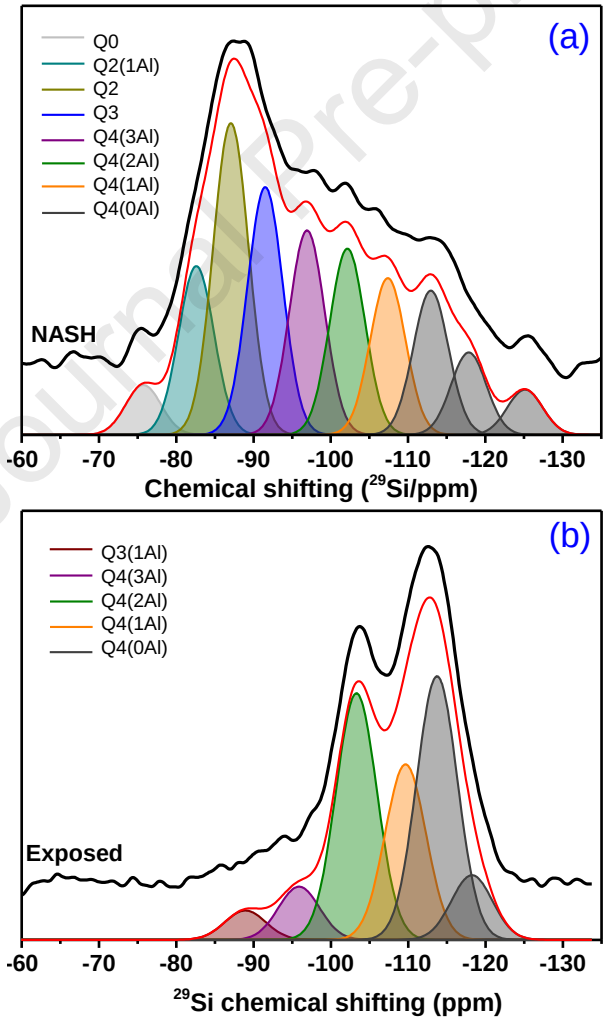

Fig. 14. ^{29}Si MAS NMR data (black lines) of (a) the unexposed NASH sample and (b) the exposed NASH sample after 28 days of sulfuric acid attack. The fitting line (red) of the spectra for the samples and associated spectral deconvolutions are also shown.

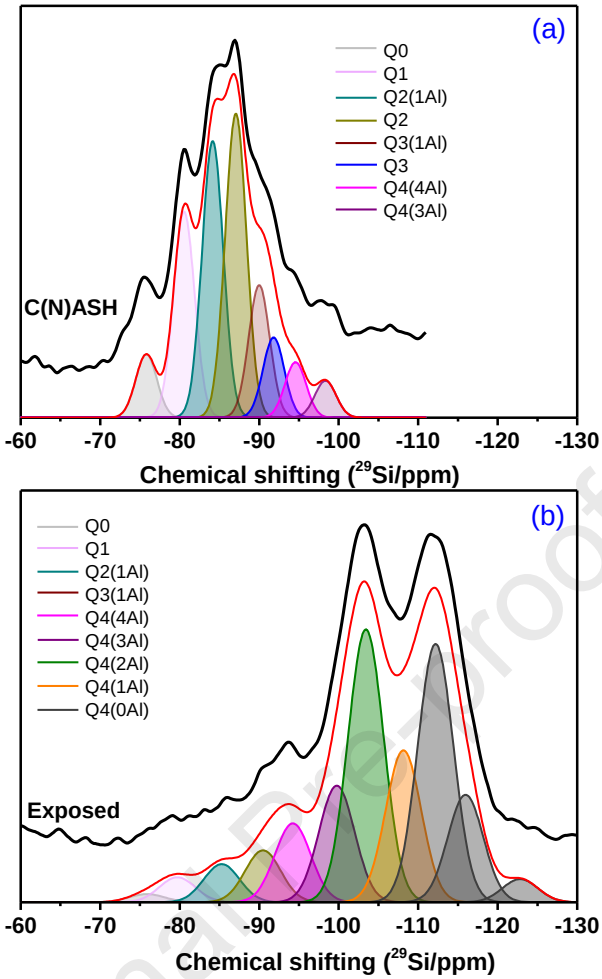

584

585 Fig. 15. ^{29}Si MAS NMR data (black lines) of (a) the unexposed C(N)ASH sample and (b) the exposed
586 C(N)ASH sample after 28 days of sulfuric acid attack. The fitting line (red) of the spectra for the
587 samples and associated spectral deconvolutions are also shown.

588

589 Table 3 Deconvolution results of ^{29}Si NMR spectra for the NASH sample and C(N)ASH sample before and after exposed to sulfuric acid. The I_A (%) is the
590 normalized relative integral area of each deconvoluted resonance in the spectra.

Sample	Coordination	Q^0	Q^1	Q^2(1Al)	Q^2	Q^3(1Al)	Q^3	Q^4(4Al)	Q^4(3Al)	Q^4(2Al)	Q^4(1Al)	Q^4(0Al)
NASH	Pos. (ppm)	-75	-	-83	-87	-	-92	-	-97	-102	-107	-113 - -125
	I_A(%)	3.1	-	10.6	19.5	-	15.5	-	12.8	11.7	9.8	17
Exposed NASH	Pos. (ppm)	-	-	-	-	-89	-	-	-96	-103	-107	-110 - -118
	I_A (%)	-	-	-	-	3.5	-	-	6.4	29.6	21.1	39.5
C(N)ASH	Pos. (ppm)	-76	-80	-84	-87	-90	-92	-95	-98	-	-	-
	I_A (%)	5.5	17.8	24.0	26.3	11.5	6.9	4.8	3.2	-	-	-
Exposed C(N)ASH	Pos. (ppm)	-76	-80	-85	-	-90	-	-94	-100	-103	-108	-112 - -123
	I_A (%)	0.7	2.2	3.4	-	4.6	-	7.0	10.3	24.1	13.4	34.3

591

4. Conclusions

In this study, stoichiometrically controlled N-A-S-H and C-(N)-A-S-H gels were used to investigate the durability properties of two typical types of AAMs under sulfuric acid attack, i.e. calcium free/low calcium AAMs (alkali-activated fly ash) and calcium bearing AAMs (alkali-activated slag). It was discovered that dealumination dominated the microstructural change of N-A-S-H gel under the sulfuric acid attack. This dealumination had minor effect on the bulk structure integrity (but not sure about the impact on micromechanical properties). The C-(N)-A-S-H gel showed both dealumination and decalcification, together with significant and rapid loss of sodium and slow loss of silicon. In addition to the normal mechanism that gypsum forms and leads to cracking at sulfuric and sulphate conditions, an important finding is that dealumination and the loss of sodium continues after decalcification and the loss of a small amount of silicon. The non-crosslinked C-(N)-A-S-H gel reduced with decrease of Si/Al ratio after exposure to sulfuric acid, while the Si/Al ratio of N-A-S-H gel increased. One common feature for the two types of AAM gels is that after acid attack, silicate polymerization degree (Q^4 concentration) increases, especially for C-(N)-A-S-H gel. Further exploration on the acid corrosion mechanism of the C-(N)-A-S-H gel could focus on the effect of Ca/Si ratio. However, the formation of coarse crystalline gypsum grains is still the controlling factor to structural destroy and needs to be controlled.

5. Acknowledgment

This work is partially supported by the National Natural Science Foundation of China (NSFC) grants (U2001225, 51878263, 51638008). The support from NSFC grant (51778003) is acknowledged as well.

Appendix I:

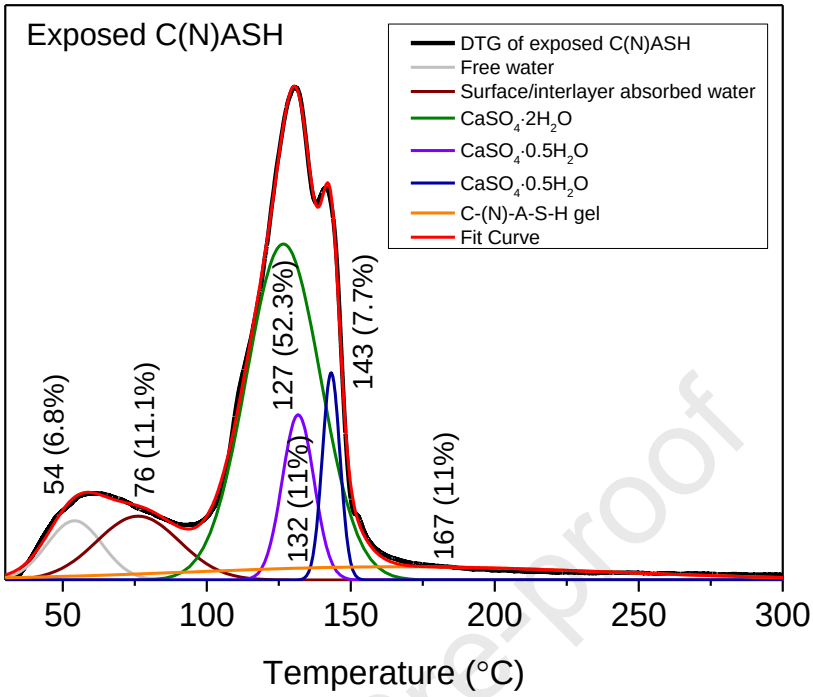

Appendix Figure 1. DTG data (black lines) of the exposed C(N)ASH binder after 28 days of sulfuric acid attack. The fitting line (red) of the spectra for the sample and associated spectral deconvolutions are also shown.

As show in the Appendix Figure 1, the $CaSO_4 \cdot 2H_2O$ accounts for around 52.3% of the weight loss of the exposed C(N)ASH sample from 90 °C to 170 °C. According to the Eq. 2, the calculated amount of $CaSO_4 \cdot 2H_2O$ is around 59.5%. The deconvoluted peaks at 132 °C and 143 °C are assigned to the decomposition of $CaSO_4 \cdot 0.5H_2O$, which account for 18.7% of the weight loss of the exposed C(N)ASH sample. The formation of two peaks is related to its different crystallinity. According to the Eq. 2 and Eq. 3, the calculated amount of $CaSO_4 \cdot 2H_2O$ is around 63.9%.

References

[1] Dyer T. Influence of cement type on resistance to attack from two carboxylic acids. Cement & Concrete Composites. 2017;83:20-35.

[2] Cao Y, Wang Y, Zhang Z, Ma Y, Wang H. Recent progress of utilization of activated kaolinitic clay in cementitious construction materials. Composites Part B: Engineering. 2021;211:108636.

[3] Grengg C, Mittermayr F, Ukrainczyk N, Koraimann G, Kienesberger S, Dietzel M. Advances in concrete materials for sewer systems affected by microbial induced concrete corrosion: A review. Water Research. 2018;134:341-52.

[4] Khan HA, Castel A, Khan MSH, Mahmood AH. Durability of calcium aluminate and sulphate resistant Portland cement based mortars in aggressive sewer environment and sulphuric acid. Cement and Concrete Research. 2019;124:105852.

[5] Aiken TA, Kwasny J, Sha W, Soutsos MN. Effect of slag content and activator dosage on the resistance of fly ash geopolymer binders to sulfuric acid attack. Cement and Concrete Research. 2018;111:23-40.

[6] Ma Y, Yang X, Hu J, Zhang Z, Wang H. Accurate determination of the "time-zero" of autogenous shrinkage in alkali-activated fly ash/slag system. Composites Part B: Engineering. 2019;177:107367.

[7] Bakharev T, Sanjayan JG, Cheng YB. Resistance of alkali-activated slag concrete to acid attack. Cement and Concrete Research. 2003;33(10):1607-11.

[8] Bernal SA, Rodríguez ED, Mejía de Gutiérrez R, Provis JL. Performance of alkali-activated slag mortars exposed to acids. Journal of Sustainable Cement-Based Materials. 2012;1(3):138-51.

[9] Cao Y, Wang Y, Zhang Z, Ma Y, Wang H. Turning sandstone clay into supplementary cementitious material: activation and pozzolanic reactivity evaluation. Composites Part B: Engineering. 2021;223:109137.

[10] Longhi MA, Rodríguez ED, Walkley B, Zhang Z, Kirchheim AP. Metakaolin-based geopolymers: Relation between formulation, physicochemical properties and efflorescence formation. Composites Part B: Engineering. 2020;182:107671.

[11] Provis JL, Van Deventer JS. State of the art report, RILEM TC 224-AAM. Springer: Springer Science & Business Media; 2014.

[12] Provis JL, Lukey GC, van Deventer JSJ. Do Geopolymers Actually Contain Nanocrystalline Zeolites? A Reexamination of Existing Results. Chemistry of Materials. 2005;17(12):3075-85.

[13] Winnefeld F, Leemann A, Lucuk M, Svoboda P, Neuroth M. Assessment of phase formation in alkali activated low and high calcium fly ashes in building materials. Construction and Building Materials. 2010;24(6):1086-93.

[14] Fernández-Jiménez A, Palomo A. Composition and microstructure of alkali activated fly ash binder: Effect of the activator. Cement and Concrete Research. 2005;35(10):1984-92.

[15] Schilling PJ, Butler LG, Roy A, Eaton HC. ^{29}Si and ^{27}Al MAS - NMR of NaOH - activated blast - furnace slag. Journal of the American Ceramic Society. 1994;77(9):2363-8.

[16] Fernández - Jiménez A, Puertas F, Sobrados I, Sanz J. Structure of calcium silicate hydrates formed in alkaline - activated slag: influence of the type of alkaline activator. Journal of the American Ceramic Society. 2003;86(8):1389-94.

[17] Taylor HF. Cement chemistry: Thomas Telford London; 1997.

[18] Myers RJ, Bernal SA, San Nicolas R, Provis JL. Generalized structural description of calcium–sodium aluminosilicate hydrate gels: the cross-linked substituted tobermorite model. Langmuir. 2013;29(17):5294-306.

[19] Pardal X, Pochard I, Nonat A. Experimental study of Si–Al substitution in calcium-silicate-hydrate (CSH) prepared under equilibrium conditions. Cement and Concrete Research. 2009;39(8):637-43.

[20] Longhi MA, Walkley B, Rodríguez ED, Kirchheim AP, Zhang Z, Wang H. New selective dissolution process to quantify reaction extent and product stability in metakaolin-based geopolymers. Composites Part B: Engineering. 2019;176:107172.

[21] Davidovits J. Geopolymers: inorganic polymeric new materials. Journal of Thermal Analysis and calorimetry. 1991;37(8):1633-56.

[22] Zhang W, Yao X, Yang T, Zhang Z. The degradation mechanisms of alkali-activated fly ash/slag blend cements exposed to sulphuric acid. Construction and Building Materials. 2018;186:1177-87.

[23] Ourgessa AW, Aniley A, Gudisa AG, Neme I, Bekele A. Effect of Alkaline Concentration and Solid Liquid Ratio on the Acid Resistance of Fly Ash Based Geopolymer Mortar. American Journal of Science, Engineering and Technology. 2019;4(4):80.

[24] Ren J, Zhang L, San Nicolas R. Degradation process of alkali-activated slag/fly ash and Portland cement-based pastes exposed to phosphoric acid. Construction and Building Materials. 2020;232:117209.

[25] Aliques-Granero J, Tognonvi T, Tagnit-Hamou A. Durability test methods and their application to AAMs: case of sulfuric-acid resistance. Materials and Structures. 2017;50(1):1-14.

[26] Shi C. Corrosion resistance of alkali-activated slag cement. Advances in Cement Research. 2003;15(2):5.

[27] Temuujin J, Minjigmaa A, Lee M, Chen-Tan N, van Riessen A. Characterisation of class F fly ash geopolymer pastes immersed in acid and alkaline solutions. Cement and Concrete Composites. 2011;33(10):1086-91.

[28] Allahverdi A, Škvára F. NITRIC ACID ATTACK ON HARDENED PASTE OF GEOPOLYMERIC CEMENTS - PART 1. Ceramics-Silikáty. 2001;45(3):8.

[29] Bernal S, Rodríguez E, Mejía de Gutiérrez R, Provis J. Performance of alkali-activated slag mortars exposed to acids. Journal of Sustainable Cement-Based Materials. 2012;1(3):138-51.

[30] Okoye FN, Prakash S, Singh NB. Durability of fly ash based geopolymer concrete in the presence of silica fume. Journal of Cleaner Production. 2017;149:1062-7.

[31] Fernández-Jiménez A, Palomo A. Characterisation of fly ashes. Potential reactivity as alkaline cements☆. Fuel. 2003;82(18):2259-65.

[32] Walkley B. Understanding geopolymers through synthetic gel systems [PhD Dessertation]. Melbourne: University of Melbourne University; 2016.

[33] Wang Y, Cao Y, Ma Y, Xiao S, Hu J, Wang H. Fresh and hardened properties of alkali-activated fly ash/slag binders: effect of fly ash source, surface area, and additives. Journal of Sustainable Cement-Based Materials. 2021:1-24.

[34] Provis JL, Myers RJ, White CE, Rose V, van Deventer JSJ. X-ray microtomography shows pore structure and tortuosity in alkali-activated binders. Cement and Concrete Research. 2012;42(6):855-64.

[35] Palomo Á, Kavalerova E, Fernández-Jiménez A, Krivenko P, García-Lodeiro I, Maltseva O. A review on alkaline activation: new analytical perspectives. 2015.

[36] Huang G, Ji Y, Zhang L, Li J, Hou Z. The influence of curing methods on the strength of MSWI bottom ash-based alkali-activated mortars: The role of leaching of OH− and free alkali. Construction and Building Materials. 2018;186:978-85.

[37] Longhi MA, Zhang Z, Walkley B, Rodríguez ED, Kirchheim AP. Strategies for control and mitigation of efflorescence in metakaolin-based geopolymers. Cement and Concrete Research. 2021;144:106431.

[38] Ye H, Huang L. Degradation mechanisms of alkali-activated binders in sulfuric acid: The role of calcium and aluminum availability. Construction and Building Materials. 2020;246:118477.

[39] Bernal SA, Rodríguez ED, Mejía de Gutiérrez R, Gordillo M, Provis JL. Mechanical and thermal characterisation of geopolymers based on silicate-activated metakaolin/slag blends. Journal of Materials Science. 2011;46(16):5477-86.

[40] Feng D, Provis JL, van Deventer JSJ. Thermal Activation of Albite for the Synthesis of One-Part Mix Geopolymers. Journal of the American Ceramic Society. 2012;95(2):565-72.

[41] Ariffin MAM, Bhutta MAR, Hussin MW, Mohd Tahir M, Aziah N. Sulfuric acid resistance of blended ash geopolymer concrete. Construction and Building Materials. 2013;43:80-6.

[42] Yang S, Du W, Shi P, Shangguan J, Liu S, Zhou C, et al. Mechanistic and kinetic analysis of Na2SO4-modified laterite decomposition by thermogravimetry coupled with mass spectrometry. PloS one. 2016;11(6):e0157369.

[43] Lothenbach B, Durdzinski P, De Weerdt K. Thermogravimetric analysis. A practical guide to microstructural analysis of cementitious materials. 2016;1.

[44] Felicetti R. Digital camera colorimetry for the assessment of fire-damaged concrete. WSp Fire design of concrete structures: what now. 2004:211-20.

[45] Hager I. Colour Change in Heated Concrete. Fire Technology. 2014;50(4):945-58.

[46] Singh M, Garg M. Making of anhydrite cement from waste gypsum. Cement and Concrete Research. 2000;30(4):571-7.

[47] Strydom CA, Hudson-Lamb DL, Potgieter JH, Dagg E. The thermal dehydration of synthetic gypsum. Thermochimica Acta. 1995;269-270:631-8.

[48] Alarcon-Ruiz L, Platret G, Massieu E, Ehrlacher A. The use of thermal analysis in assessing the effect of temperature on a cement paste. Cement and Concrete Research. 2005;35(3):609-13.

[49] Svinning K, Høskuldsson A, Justnes H. Prediction of compressive strength up to 28days from microstructure of Portland cement. Cement and Concrete Composites. 2008;30(2):138-51.

[50] Rees CA, Provis JL, Lukey GC, van Deventer JSJ. Attenuated Total Reflectance Fourier Transform Infrared Analysis of Fly Ash Geopolymer Gel Aging. Langmuir. 2007;23(15):8170-9.

[51] Zhang Z, Wang H, Provis JL, Bullen F, Reid A, Zhu Y. Quantitative kinetic and structural analysis of geopolymers. Part 1. The activation of metakaolin with sodium hydroxide. Thermochimica Acta. 2012;539:23-33.

[52] Bernal SA, Mejía de Gutiérrez R, Pedraza AL, Provis JL, Rodriguez ED, Delvasto S. Effect of binder content on the performance of alkali-activated slag concretes. Cement and Concrete Research. 2011;41(1):1-8.

[53] Walkley B, San Nicolas R, Sani M-A, Rees GJ, Hanna JV, van Deventer JSJ, et al. Phase evolution of C-(N)-A-S-H/N-A-S-H gel blends investigated via alkali-activation of synthetic calcium aluminosilicate precursors. Cement and Concrete Research. 2016;89:120-35.

[54] Lane MD. Mid-infrared emission spectroscopy of sulfate and sulfate-bearing minerals. American Mineralogist. 2007;92(1):1-18.

[55] García-Lodeiro I, Fernández-Jiménez A, Blanco MT, Palomo A. FTIR study of the sol–gel synthesis of cementitious gels: C–S–H and N–A–S–H. Journal of Sol-Gel Science and Technology. 2008;45(1):63-72.

[56] Król M, Rożek P, Chlebda D, Mozgawa W. Influence of alkali metal cations/type of activator on the structure of alkali-activated fly ash – ATR-FTIR studies. Spectrochimica Acta Part A: Molecular and Biomolecular Spectroscopy. 2018;198:33-7.

[57] Duxson P, Lukey GC, Separovic F, van Deventer JSJ. Effect of Alkali Cations on Aluminum Incorporation in Geopolymeric Gels. Industrial & Engineering Chemistry Research. 2005;44(4):832-9.

[58] Walkley B, Provis JL. Solid-state nuclear magnetic resonance spectroscopy of cements. Materials Today Advances. 2019;1:100007.

[59] Gao X, Yu QL, Brouwers HJH. Apply 29Si, 27Al MAS NMR and selective dissolution in identifying the reaction degree of alkali activated slag-fly ash composites. Ceramics International. 2017;43(15):12408-19.

Conflicts of Interest

The authors declare no conflict of interest on this manuscript entitled with “Study of acidic degradation of alkali-activated materials using synthetic C-(N)-A-S-H and N-A-S-H gels”.

The authors were listed as follow,

Yanru Wang, Yubin Cao, Zuhua Zhang, Jizhong Huang, Peng Zhang, Yuwei Ma, Hao Wang.